Constraints on the symmetry energy from heavy ion collisions

W.G. Lynch[1,2], M.B. Tsang[1,2], Z. Chajecki[1], D. Coupland[1], P. Danielewicz[1,2], M. Famiano[1], R. K. Hodges[1], M. Kilburn[1], F. Lu[2,4], J. Winkelbauer[1], M. Youngs[1], Y.Z. Zhang[5]

[1]*National Superconducting Cyclotron Laboratory & Department of Physics and Astronomy, Michigan State University, East Lansing, MI 48824, USA*

[2]*Joint Institute of Nuclear Astrophysics, MSU, East Lansing, Michigan 48824, USA*

[3]*Department of Physics, Western Michigan University, Kalamazoo, Michigan 49008, USA*

[4]*Department of Physics and State Key Laboratory of Nuclear Physics and Technology, Peking University, Beijing 100871, China*

[5]*China Institute of Atomic Energy, P.O. Box 275 (18), Beijing 102413, China*

. * *email: lynch@nscl.msu.edu*

Constraints on the Equation of State for symmetric matter (equal neutron and proton numbers) have been extracted from energetic collisions of heavy ions over a range of energies. Collisions of neutron-deficient and neutron-rich heavy ions now provide initial constraints on the Equation of State of neutron-rich matter at sub-saturation densities from isospin diffusions and neutron proton ratios. This talk reviews the experimental constraints from heavy ion reactions on the density dependence of symmetry energy at sub-saturation density. These constraints are compared to other available constraints from nuclear structures, masses and neutron skins.

1. Introduction

The Equation of State (EoS) of cold nuclear matter can be written as the sum of the energy per nucleon of symmetric matter and a symmetry energy term, E_δ,

$$E(\rho,\delta) = E_0(\rho,\delta=0) + E_\delta ; E_\delta = S(\rho,\delta^2) \quad (1)$$

where $\delta=(\rho_n-\rho_p)/\rho$ is the asymmetry; $S(\rho)$ describes the density dependence of E_δ ρ_n, ρ_p and ρ are the neutron, proton and nucleon densities, respectively. The first term on the RHS, $E_0(\rho,\delta=0)$ is the EoS term for symmetric nuclear matter with equal fractions of neutrons and protons. Heavy ion collision measurements have constrained $E_0(\rho,\delta=0)$ for densities ranging from $\rho_0 \leq \rho \leq 5\rho_0$ [1,2]. Until recently, well-determined constraints on the symmetry term, E_δ, are few.

Macroscopic quantities of asymmetric nuclear matter exist over a wide range of densities in neutron stars and in type II supernovae [3]. Experimental information about the asymmetry term in the EoS can improve predictions for neutron star observables such as stellar radii and moments of inertia, crustal vibration frequencies [4,5], and neutron star cooling rates [4,6] that are currently being investigated with ground-based and satellite observatories. For many of these observables, the absence of strong constraints on the symmetry energy term of the EoS engenders major theoretical uncertainties. Consequently, determining the EoS has been a major motivation for many X-ray observations of neutron stars including the proposed International X-ray Observatory [7]. In Nuclear Physics, investigations that provide an improved understanding of E_δ will greatly improve our description of nuclear masses [8], fission barriers, energies of isovector collective vibrations [9], and the role of isovector modes in fusion and strongly damped collisions as well as the neutron skins of neutron-rich nuclei [10].

This talk focuses on investigations of the symmetry energy at sub-saturation density, where nucleus-nucleus collisions provide constraints to the symmetry energy using different experimental observables. The resulting constraints are compared to constraints obtained from nuclear structure studies. Finally, recent planned efforts to provide constraints on

the symmetry energy and the EoS for neutron-rich matter over a broad range of densities will be discussed.

2. Experimental observables from heavy ion collisions

Large variations in nuclear density can be attained momentarily in nuclear collisions, and constraints on the Equation of State (EoS) can be obtained by comparing measurements to transport calculations of such collisions. Significant constraints on the symmetric matter EoS at $1 \le \rho/\rho_0 \le 4.5$ have been obtained from measurements of collective flow [1] and Kaon production [2]. The symmetry energy has been recently probed at sub-saturation densities via isospin diffusion [11,12], and by double ratios involving neutron and proton energy spectra [13]. These two observables largely reflect the transport of nucleons under the combined influence of the mean fields and the collisions induced by residual interactions; thus, they should be within the predictive capabilities of transport theory. In the following, we compare both observables to the predictions from the Improved Quantum Molecular Dynamics (ImQMD) transport model, and obtain consistent constraints on the symmetry energy at sub-saturation densities. These constraints are then compared to the results obtained from Isobaric Analog States, Sn isotope skins, Pb neutron skin thickness, results from Pygmy Dipole Resonance and the Giant Dipole Resonance experiments.

3. ImQMD: Transport calculations for heavy ion collisions

Transport models have been used to describe the dynamics of heavy ion collisions. We chose to use the Quantum Molecular Dynamic (QMD) model mainly because of its ability to describe fragments which are quite important in describing isospin observables. In the QMD model, nucleons are represented by Gaussian wave packets, and the mean fields acting on these wave packets are derived from an energy functional with the potential energy U that includes the full Skyrme potential energy with just the spin-orbit term omitted:

$$U = U\rho + U_{md} + U_{coul} \quad (2)$$

where U_{coul} is the Coulomb energy. The nuclear contributions are represented in a local form with

$$U_{\rho,md} = \int u_{\rho,md}\, d^3r$$

and,

$$u_\rho = \frac{\alpha}{2}\frac{\rho^2}{\rho_0} + \frac{\beta}{\eta+1}\frac{\rho^{\eta+1}}{\rho_0^{\eta}} + \frac{g_{sur}}{2\rho_0}(\nabla\rho)^2 + \frac{g_{sur,iso}}{\rho_0}[\nabla(\rho_n - \rho_p)]^2 + \frac{C_s}{2}\left(\frac{\rho}{\rho_0}\right)^{\gamma}\delta^2\rho + g_{\rho\tau}\frac{\rho^{8/3}}{\rho_0^{5/3}} \quad (3)$$

where the asymmetry

$$\delta = (\rho_n - \rho_p)/(\rho_n + \rho_p),$$

and ρ_n and ρ_p are the neutron and proton densities, respectively. A symmetry kinetic energy density of the form $\frac{C_{s,k}}{2}\left(\frac{\rho}{\rho_0}\right)^{2/3}\delta^2\rho$ and symmetry potential energy density of the form $\frac{C_{s,p}}{2}\left(\frac{\rho}{\rho_0}\right)^{\gamma}\delta^2\rho$ were used in the improved version of the QMD code (ImQMD). The energy density associated with the mean-field momentum dependence is represented by

$$u_{md} = \frac{1}{2\rho_0}\sum_{N_1,N_2=n,p}\frac{1}{16\pi^6}\int d^3p_1 d^3p_2 f_{N_1}(\vec{p}_1) f_{N_2}(\vec{p}_2)\, 1.57\left[\ln\left(1+5\times10^{-4}(\Delta p)^2\right)\right]^2 \quad (4)$$

where f_N are nucleon Wigner functions, $\Delta p = |\vec{p}_1 - \vec{p}_2|$, the energy is in MeV and momenta are in MeV/c. The resulting interaction between wavepackets is described in Ref. [14]. Unless otherwise noted, we use α= -356 MeV, β =303 MeV and η=7/6, corresponding to a isoscalar compressibility constant of K=200 MeV, and g_{sur}=19.47 MeVfm^2, g_{suriso}=-11.35

MeVfm^2, $C_{s,k}$=24.9 MeV, $C_{s,p}$=35.19 MeV, and $g_{\rho\tau}$=0 MeV.

These calculations use isospin-dependent in-medium nucleon-nucleon scattering cross sections in the collision term and Pauli blocking effects that are described in [15,16,17]. Cluster yields are calculated by means of the coalescence model widely used in QMD calculations in which particles with relative momenta smaller than P_0 and relative distances smaller than R_0 are coalesced into one cluster. In the present work, values of R_0= 3.5 *fm* and P_0=250 MeV/c are employed.

4. Experimental constraints from heavy ion collisions

We turn our attention first to the interpretation of neutron/proton double ratio data, which derives its sensitivity to the symmetry energy from the opposite sign of the symmetry force for neutrons as compared to protons [18]. First experimental comparisons of neutron and proton spectra in Ref. [13] used a double ratio in order to reduce sensitivity to uncertainties in the neutron detection efficiencies and to relative uncertainties in energy calibrations of neutrons and protons. This double ratio,

$$DR(n/p) = Rn/p(A)/\ Rn/p(B) = \frac{dM_n(A)/dE_{c.m.}}{dM_p(A)/dE_{c.m.}} \cdot \frac{dM_p(B)/dE_{c.m.}}{dM_n(B)/dE_{c.m.}} \qquad (5)$$

was constructed by measuring the energy spectra, $dM/dE_{c.m}$, of neutrons and protons for two systems A and B characterized by different isospin asymmetries. The star symbols in the left panel of Figure 1 show the neutron-proton double ratios measured at $70° \le \theta_{CM} \le 110°$ as a function of center-of-mass (c.m.) energy for nucleons for central collisions of ^{124}Sn+^{124}Sn and ^{112}Sn+^{112}Sn at E/A=50 MeV.

We have performed calculations at an impact parameter of b=1, 2 and 3 fm at an incident energy of 50 MeV per nucleon for two systems: A=^{124}Sn+^{124}Sn and B=^{112}Sn+^{112}Sn. About 60,000 events are simulated for each impact parameter. Within the statistical uncertainties, the double ratio observable, DR(n/p), is nearly independent of the impact parameters within the range of $0 \le b \le 5$ *fm*. The lines in the left panel of Figure 1 show the

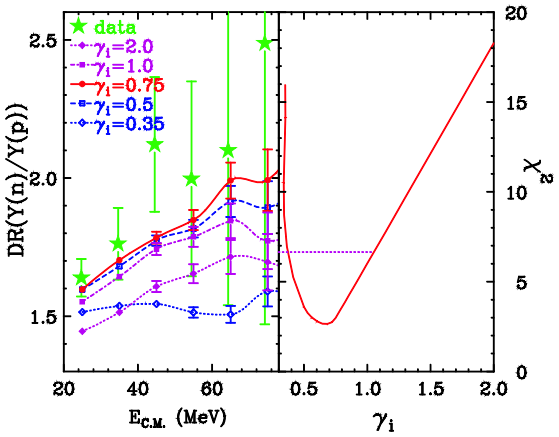

Fig.1: Left panel: Comparison of experimental double neutron-proton ratios (star symbols), as a function of nucleon center of mass energy, to ImQMD calculations (lines) with different density dependence of the symmetry energy parameterized in terms of γ_i in Eq. (3). Right panel: A plot of χ^2 as a function of γ_i.

predicted double ratios DR(np) as a function of the center of mass energy of nucleons emitted at $70° \le \theta_{c.m.} \le 110°$ for γ_i = 0.35, 0.5, 0.75, 1 and 2. The uncertainties for these calculations in Figure 1 are statistical. As fewer nucleons are emitted at high energy, the uncertainties increase with increasing energy. Despite the large experimental uncertainties, especially for the higher energy (> 40 MeV) data, the trends and magnitudes of the data points definitely rule out the very soft (γ_i =0.35, dotted line with open diamond points) and very stiff (γ_i =2, dotted line with closed diamond symbols) density-dependent symmetry terms. The right panel shows the total χ^2 computed from the difference between predicted and measured double ratios as a function of γ_i. We find the 2σ uncertainty range of values for γ_i to be $0.4 \le \gamma_i \le$ to 1.4, corresponding to an increase in χ^2 by 4 above its minimum of $\chi^2 \sim 2.1$ near γ_i =0.7.

The density dependence of the symmetry energy can also be probed in peripheral collisions between two nuclei with different

isospin asymmetries by examining the diffusion of neutrons and protons across the neck that joins the nuclei. This "isospin diffusion" generally continues until the two nuclei separate or until the chemical potentials for neutrons and protons in both nuclei become equal. To isolate diffusion effects from other effects such as pre-equilibrium emission, Coulomb effects, and secondary decays, measurements of isospin diffusion compare "mixed" collisions involving a neutron-rich nucleus A and a neutron-deficient nucleus B to the "symmetric" collisions involving A+A and B+B. The degree of isospin equilibration in such collisions can be quantified by rescaling the isospin observable X according to the isospin transport ratio $R_i(X)$ [11] given by

$$R_i(X) = 2\frac{X - (X_{A+A} + X_{B+B})/2}{X_{A+A} - X_{B+B}} \quad (6)$$

In the absence of isospin diffusion, $R_i(X_{A+B}) = R_i(X_{A+A}) = 1$ for a collision involving a neutron-rich projectile on a proton-rich target. Likewise, without diffusion, $R_i(X_{B+B}) = R_i(X_{B+A}) = -1$. On the other hand, if isospin equilibrium is achieved for roughly equal sized projectiles and target nuclei, $R_i(X_{A+B}) = R_i(X_{B+A}) = 0$.

Eq. (6) dictates that different observables, X, provide the same results if they are linearly related [12]. Experimental isospin transport ratios obtained from isoscaling parameters, α, [11] and from yield ratios of A=7 mirror nuclei, $R_7 = R_i(X_7 = ln(Y(^7Li)/Y(^7Be)))$ are consistent, i.e. $R_i(\alpha) \cong R_7$, reflecting linear relationships between α, X_7, and the asymmetry δ of the emitting source [12]. For emission at a specific rapidity y, we assume $R(\alpha)=R(\delta)=R_7$ to be valid, as has been confirmed experimentally [12,18] and theoretically for all statistical and dynamical calculations [18,19,20]. We calculate δ from the asymmetry of the fragments and free nucleons emitted at the relevant rapidity, but our conclusions do not significantly change if fragments alone are used to calculate δ.

Experimental isospin diffusion transport ratios, $R_i(\alpha)$, plotted as shaded regions in the left panel of Figure 2, have been obtained using Eq. (6) with isoscaling data at $y/y_{beam} \geq 0.7$ from $^{124}Sn+^{112}Sn$ (top region) and $^{112}Sn+^{124}Sn$ (bottom region) scaled by the symmetric collisions of $^{124}Sn+^{124}Sn$, $^{112}Sn+^{112}Sn$ [12]. We have performed ImQMD calculations at impact parameters of b=5, 6, 7, and 8 fm. The lines in the left panel of Figure 2 show the predicted isospin transport ratio $R_i(\delta)$ as a function of impact parameter b for γ_i=0.35, 0.5, 0.75, 1 and 2. At sub-saturation densities, larger symmetry energies (and faster equilibration) occur for smaller γ_i values in isospin diffusion. Thus we see a monotonic decrease of $R_i(\delta)$ with decreasing γ_i. Cross-section estimates suggest that the isospin diffusion data cover the impact parameter range of 5.8 to 7.5 fm [12] and the data primarily reflects contributions from impact parameters of b=6 to 7 fm. We have performed the χ^2 analysis for both impact parameters in the right panel of Figure 2. Compared to Fig. 1, the χ^2 minima are lower; using the same 2σ criterion, the analysis brackets the region $0.4 \leq \gamma_i \leq 1.0$.

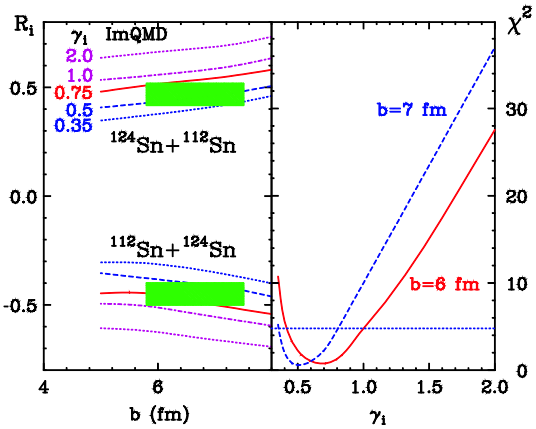

Fig. 2: Left panel: Comparison of experimental isospin transport ratios [11] (shaded regions) to ImQMD results (lines), for different impact parameters. Right panel: χ^2 analysis for b=6 fm (solid curve) and b=7 fm (dashed curve) as a function of γ_i.

ImQMD calculations provide predictions for fragment yields as a function of rapidity at b=6 fm as shown by the lines in the left panel of Figure 3. The star symbols represent measured values of R_7 obtained from the yield ratios of ^{7}Li and ^{7}Be, [12]. This calculation of the shapes and

magnitude of the rapidity dependence of the isospin transport ratios R_7 reproduces the trends accurately. The corresponding χ^2 analysis at b=6 (solid curve) and 7 (dashed curve) fm in the right panel displays sharp minima. Using the 2σ criterion adopted previously, the analysis favors the region $0.45 \leq \gamma_i \leq 0.95$.

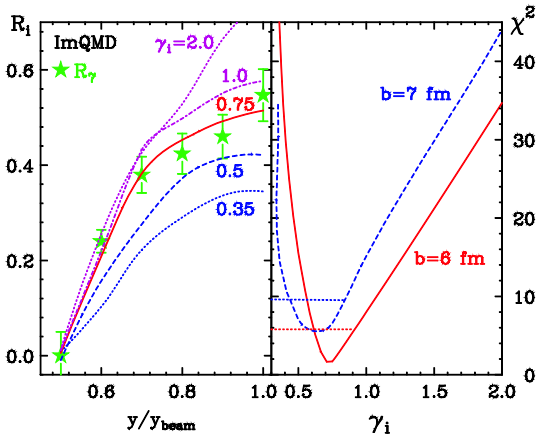

Fig. 3 : Left panel: Comparison of experimental isospin transport ratios obtained from the yield ratios of A=7 isotopes [12] (star symbols), as a function of the rapidity, ImQMD calculations (lines) for b=6 fm. Right panel: χ^2 analysis for b=6 fm (solid curve) and b=7 fm (dashed curve) as a function of γ_i.

More recently, isospin diffusion measurements have been carried out at E/A=35 MeV [21]. At lower incident energy, due to longer contact time, it is expected that the system will become more equilibrated in the isospin degree of freedom. Figure 4 compares the measured isospin transport ratios for reduced impact parameter, $\hat{b}$=0.1 (open circle), 0.23(open square), 0.34(open diamond), 0.46 (open triangle), 0.58 (open star) to predictions from the ImQMD models (lines). The left panel shows the comparison for a softer symmetry energy with γ_i=0.5 and the right panel shows the comparison for a stiffer symmetry energy with γ_i=2.0. Both calculations and experiment predict impact parameter independent values for the isospin transport ratios at central collisions. Similar to the results at E/A=50 MeV, the isospin transport ratios are better reproduced by the softer symmetry energy with γ_i=0.5.

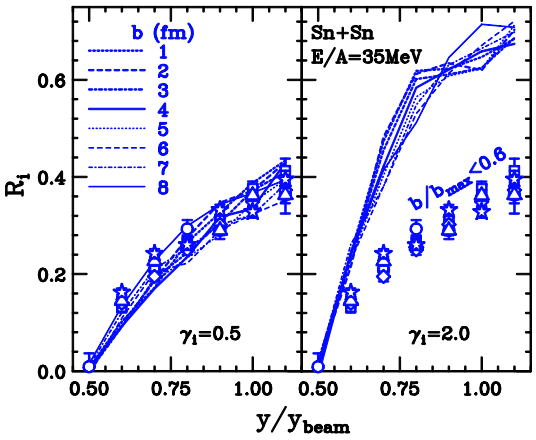

Figure 4: Left panel: Isospin transport ratios plotted as a function of the normalized rapidity. The lines are ImQMD calculations using the softer symmetry potential with γ_i=0.5. Right panel: Same as left panel but with a stiffer symmetry potential of γ_i=2.0 is used in the calculation. The symbols in both panels are data with different reduced impact parameter cut.

5. Experimental Comparison at sub-saturation density

There are substantial overlaps between the constraints obtained from isospin diffusion and double neutron and proton yield ratios as shown in Figures 1, 2 and 3. Many recent efforts to constrain the density dependence of the symmetry energy have focused on its behavior near saturation density. There, one may expand the symmetry energy, S(ρ), about the saturation density, ρ_o,

$$S(\rho) = S_0 + \frac{L}{3}\left(\frac{\rho-\rho_0}{\rho_0}\right) + \frac{K_{sym}}{18}\left(\frac{\rho-\rho_0}{\rho_0}\right)^2 + \ldots \quad (7)$$

where L and K_{sym} are slope and curvature parameters at ρ_o. K_{sym} is strongly correlated to L [22]. As the second term in Eq. (4) is much larger than the third term, we believe L can be determined more reliably than. K_{sym}. The slope parameter, L, is related to p_o, the pressure from

the symmetry energy for pure neutron matter at saturation density:

$$L = 3\rho_0 |dS(\rho)/d\rho|_{\rho_0} = [3/\rho_0] \cdot P_0 \quad (8)$$

p_o, provides the baryonic contribution to the pressure in pure neutron matter at saturation density [6], where the energy of symmetric matter, $E_o(\rho, \delta=0)$ does not contribute to the pressure. It is also related to the neutron skin thickness, δR_{np}, of neutron-rich heavy nuclei including ^{208}Pb [23,24].

Constraints on the exponent γ_i depend on the symmetry energy at saturation density, $S_0 = S(\rho_0)$. Increasing S_0 has the same effect on the isospin transport ratio as decreasing γ_i. Thus S_0 and L cannot be determined independently. To provide constraints on S_0 and L parameters, contours with constant χ^2 values can be created by doing two-dimensional χ^2 analysis in the γ_i - S_0 parameter space. We have preformed a series of ImQMD calculations at b=6 fm with different values of γ_i over selected values of S_0 between 25 to 40 MeV to locate the approximate boundaries in the S_0 and L plane that satisfy the 2σ criterion in the χ^2 analysis of the isospin diffusion data. The area bounded by the two solid diagonal lines in Figure 5 and the shaded region in Figure 6 represents a conservative estimate in such effort. Another independent constraint will be needed to provide constraints in S_0 or L.

Recent analysis of the skin thickness of tin isotopes [25, 22] suggests that L decreases with increasing S_0. The two diagonal dashed lines plotted in Figure 5 represent a 2σ analysis of the χ^2 using the Sn skin thickness data. Since the trend is opposite to that of the constraints provided by the heavy ion reactions (solid lines), the overlap of the two constraints provide a range of S_0 or L values. As pointed out by Chen et al, the interesting thing to note is that the mean L values, represented by the horizontal line in Figure 5 obtained from the overlap region of the two constraints, are nearly constant. The range of L and S_0 values in the overlap region corresponds to a mean skin thickness of ^{208}Pb of about 0.18 ± 0.04 *fm* [6]. The range of experimental neutron skin thicknesses varies from about 0.13 to 0.22 *fm* [26,27,28,29,30] which are consistent with results predicted by the constraints.

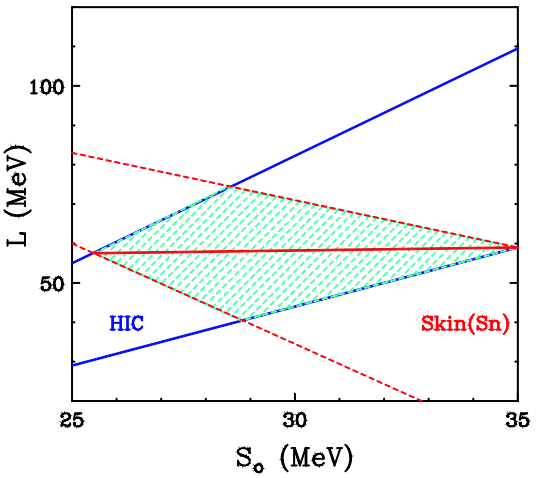

Fig. 5: Representation of the constraints on the density dependence of symmetry energy as a function of the symmetry energy at saturation density in neutron matter. The two solid lines are the boundary obtained using 2σ criteria in the χ^2 analysis of the data shown in Figures 1, 2 and 3. The two dashed lines represent the constraint boundaries obtained from the analysis of the skin thickness of tin isotopes [25, 22]. The hatched represent the overlap of these two constraints. The horizontal line indicates the nearly constant mean L value in the overlap region.

In Figure 6, we have included other attempts to extract the symmetry energy from the properties of individual nuclei. The corresponding values of pure neutron matter pressure, p_0, are given in the right axis. The lower box centered at S_0 = 32.5 MeV depicts the range of S_0 and ρ_o values from analyses of low-lying electric dipole strength (Pygmy Dipole Resonance, PDR) in neutron-rich nuclei ^{68}Ni and ^{132}Sn [9, 31]. The upper box centered at S_0 = 32.5 MeV depicts the constraints reported in Ref. [22] from the analyses of the excitation energies of Isobaric Analog States (IAS). All these constraints overlap significantly with the hatched

regions obtained from the heavy ion collisions of tin isotopes as described in section 3 and 4. The inset shows what this analysis implies about the density dependence of the symmetry energy. A value for the symmetry energy at around 0.6 normal nuclear matter density, extracted from Giant Dipole Resonance (GDR) data [32], is indicated by the symbol in the inset. It lies within the heavy ion constraints.

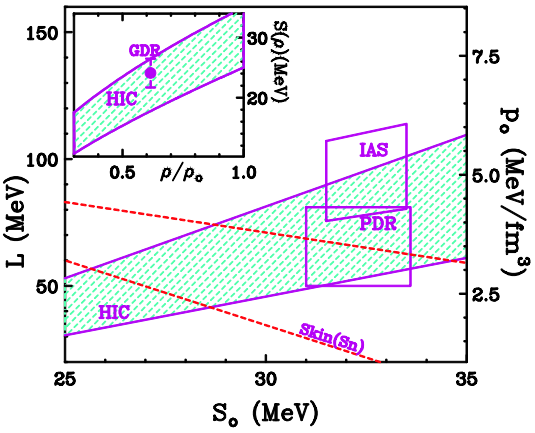

Fig. 6 : Comparison of various constraints on the density dependence of symmetry energy (inset) and pressure as a function of the symmetry energy at saturation density in neutron matter. The hatched areas are extracted from recent analyses of nuclear collisions of Sn nuclei. Open rectangles and the symbol in the inset were obtained from the properties of individual nuclei.

6. Summary and outlook

In summary, the ability of QMD models to reproduce both isospin diffusion data and double ratio of neutron and proton spectra is an important step forward in obtaining information about the symmetry energy in heavy-ion collisions. The heavy ion observables examined here provide consistent constraints on the density dependence of the symmetry energy. Some shifts in the boundaries of the constraints can be expected with improvements in the precision of experimental data and in the understanding of the transport models. Similarly there will be shifts of the constraints provided by the other observables as better data and calculations become available. Nevertheless, the consistency between the different probes of the symmetry energy suggests that increasingly stringent constraints on the symmetry energy at sub-saturation density can be expected.

To explore the density dependence of the symmetry energy over a wide range of nuclear density, an international collaboration, called the Symmetry Energy Project, SEP, consisting of an interdisciplinary, experimental and theoretical team of scientists, has been formed [33] to conduct a series of experiments at unique facilities based in the U.S. (the National Superconducting Cyclotron Laboratory at Michigan State University), Japan (the Radioactive Ion Beam Factory at RIKEN) and GSI, Germany. Each facility enables the exploration of a different density range. With experiments underway at GSI, better constraints at supra normal density is expected in the near future.

Acknowledgement

This work has been supported by the U.S. National Science Foundation under Grants PHY-0216783, 0456903, 0606007, 0800026, and the Chinese National Science Foundation of China under Grants 10675172, 10175093, 10235030.

References

[1] P. Danielewicz, W.G. Lynch, R. Lacey, Science 298, 1592 (2002).
[2] C. Fuchs, Prog. Part. Nucl. Phys. 56, 1, (2006).
[3] J. M. Lattimer and M. Prakash, Astrophys. J., 550, 426 (2001).
[4] J. M. Lattimer and M. Prakash, Science 304, 536 (2004).
[5] A. R. Villarreal and T. E. Strohmayer, Astrophys. J. **614, L121** (2004).
[6] A. W. Steiner, Phys. Rep. 411, 325 (2005).
[7] http://ixo.gsfc.nasa.gov/science/goals.html
[8] P. Danielewicz, Nucl. Phys. A727, 233 (2003).
[9] A. Klimkiewicz et al., Phys. Rev. C 76, 051603 (2007).
[10] B. A. Brown, Phys. Rev. Lett. 85, 5296 (2000).

[11] M. B. Tsang et al., Phys. Rev. Lett. 92, 062701 (2004).
[12] T. X. Liu et al., Phys. Rev. C 76, 034603 (2007).
[13] M. A. Famiano et al., Phys. Rev. Lett. 97, 052701 (2006).
[14] J. Aichelin et al., Phys. Rev. Lett. 58, 1926 (1987).
[15] Y. Zhang and Z. Li, Phys. Rev. C 71, 024604 (2005).
[16] Y. Zhang and Z. Li, Phys. Rev. C 74, 014602 (2006).
[17] Y. Zhang, Z. Li and P. Danielewicz, Phys. Rev. C 75, 034615 (2007).
[18] M. B. Tsang et al., Phys. Rev. Lett. 86, 5023 (2001).
[19] A. S. Botvina et al., Phys. Rev. C 65, 044610 (2002).
[20] A. Ono et al., Phys. Rev. C 68, 051601(R) (2003).
[21] Z. Sun et al., Phys. Rev. C in press (2010).
[22] P. Danielewicz and Jenny Lee *Nucl. Phys. A* 818, 36 (2009).
[23] C. J. Horowitz et al., Phys. Rev. Lett. 86, 5647 (2001).
[24] S. Typel and B. A. Brown, Phys. Rev. C 64, 027302 (2001).
[25] L.W. Chen et al., *Phys. Rev.* C 82 024321(2010).
[26] A. Krasznahorkay et al., Nuc. Phys. A567, 521 (1994).
[27] L. Ray, Phys. Rev. C 19, 1855 (1979).
[28] S. Karataglidis et al., Phys. Rev. C 65, 044306 (2002).
[29] B. Klos et al., Phys. Rev. C 76, 014311 (2007).
[30] V. E. Starodubsky and N. M. Hintz, Phys. Rev. C 49, 2118 (1994).
[31] Andrea Carbone et. al, Phys. Rev. C 81, 041301(R) (2010).
[32] Luca Trippa et al., Phys. Rev. C 77, 061304(R) (2008).
[33] http://groups.nscl.msu.edu/hira/sep.htm.